行政院國家科學委員會專題研究計畫　成果報告

側向振動梳狀微結構流場阻尼之數值計算

計畫類別：個別型計畫
計畫編號：NSC92-2212-E-032-009-
執行期間：92 年 08 月 01 日至 93 年 07 月 31 日
執行單位：淡江大學航空太空工程學系(所)

計畫主持人：陳慶祥

報告類型：精簡報告

處理方式：本計畫可公開查詢

中　華　民　國 93 年 10 月 5 日

行政院國家科學委員會專題研究計畫成果報告
側向振動梳狀微結構流場阻尼之數值計算
Numerical Simulation of Damping in the Flow Field of Laterally Driven Micro Comb Structures

計畫編號：NSC 92-2212-E-032-009
執行期限：92 年 8 月 1 日至 93 年 7 月 31 日
主持人：陳慶祥　　執行機構：淡江大學航太系

中文摘要

本文以數值方法求解 Navier-Stokes 方程組來模擬側向振動梳狀微結構流場，數值計算所得之品質因子與實驗結果相當吻合。數值結果顯示作簡諧運動的結構底面的阻尼約為全部阻尼的 66%，此一數值與 Couette flow 模型所計算結果相當吻合，上表面、側表面及前表面之阻尼各約為全部的 10-12%。滑動效應會減少約 7%的下表面阻尼。

關鍵詞：梳狀微結構、黏滯阻尼、數值模擬

Abstract

The Navier-Stokes simulation was used to simulate two laterally driven micro comb structures in this study. The total quality factors predicted numerically agree quite well with the experimental data. The numerical results show that the bottom surface of the oscillating structure contributes about 66% of the total damping and is very close to that predicted by the Couette flow model [1]. The top, side, and edge surface each contributes about 10-12%. The slip effect was also included in this study. The slip effect reduces the viscous damping on the bottom surface of the oscillating structure by about 7%.

Keywords: Micro Comb Structure, Viscous Damping, Numerical Simulation

I. Introduction

Among the factors that affect the dynamic performance of a resonant sensor, such as mass, resonant frequency, stiffness, and damping, damping is the most difficult to estimate. This is because there are several damping mechanisms related to the total Q, for example, viscous and acoustic dampings, damping due to imbalance in the structure, and damping resulting from internal material related losses [2]. Viscous damping due to the interaction between the vibrating structure and the surrounding fluid (mostly air) is the dominant damping mechanism in most resonant sensors. Yet, it is the most difficult to estimate accurately, because the flow is highly nonlinear.

Figure 1 shows a typical laterally driven micro comb structure, consisting of a mass suspended with tethers anchored onto the sensor body. The lateral motion of the vibrating structure alters the distance between the capacitor and changes the output voltage. To maintain system sensitivity, the stiffness of the supporting tethers should be kept small.

II. Numerical solutions

The non-dimensional boundary conditions are

(1). $\bar{u} = \bar{v} = 0$, on the surfaces of fixed structures

(2). $\bar{u} = \cos\tau$, $\bar{v} = 0$, on the surfaces of the oscillating structure

(3). $\dfrac{\partial \bar{u}}{\partial \bar{y}} = \dfrac{\partial \bar{v}}{\partial \bar{y}} = 0, \quad \bar{p} = 0,$ as $\bar{y} \to \infty$

(4). $\dfrac{\partial \bar{u}}{\partial \bar{x}} = \dfrac{\partial \bar{v}}{\partial \bar{x}} = \dfrac{\partial \bar{p}}{\partial \bar{x}} = 0,$ on the

right and left boundaries
(5). the slip boundary conditions were used if the slip flow was assumed.
The mean free path, λ, of the air under standard atmospheric conditions is about $0.06\,\mu m$, $\mu = 10^{-6}$. The gap d between the oscillating structure and the substrate for a typical micro comb structure is about $2\,\mu m$. The Knudsen number in region II is $Kn = \lambda / d = 0.03$, which indicates that the flow is in the slip flow region and the slip effect must be taken into account. For slip flows, the fluid can be assumed to be a continuum but the slip boundary condition must be utilized to account for the incomplete momentum exchange between the gas molecules and the walls. The slip boundary condition on the bottom surface of the oscillating structure is

$$\bar{u}_w = -\frac{2-\sigma}{\sigma} Kn(\frac{\partial \bar{u}}{\partial \bar{y}})_w + \cos\tau$$

The parameter σ is the ratio of diffusively reflected molecules from the wall. The slip boundary condition on the substrate surface is

$$\bar{u}_w = \frac{2-\sigma}{\sigma} Kn(\frac{\partial \bar{u}}{\partial \bar{y}})_w$$

We assumed that σ =1 in this study. The slip boundary conditions were applied in region II within the left and right edges of the oscillating structure.

To simulate the motion of the oscillating structure, the computations were conducted on the transformed coordinate system (ξ,η), where $\bar{x} = \bar{x}(\xi), \bar{y} = \bar{y}(\eta)$. The transformed governing equations are

$$\frac{1}{\bar{x}_\xi}\frac{\partial \bar{u}}{\partial \xi} + \frac{1}{\bar{y}_\eta}\frac{\partial \bar{v}}{\partial \eta} = 0 \qquad (1)$$

$$St \cdot \mathrm{Re}\frac{\partial \bar{u}}{\partial \tau} + \mathrm{Re}(\bar{u}\frac{1}{\bar{x}_\xi}\frac{\partial \bar{u}}{\partial \xi} + \bar{v}\frac{1}{\bar{y}_\eta}\frac{\partial \bar{u}}{\partial \eta})$$
$$= -\frac{1}{\bar{x}_\xi}\frac{\partial \bar{p}}{\partial \xi} + [\frac{1}{\bar{x}_\xi}\frac{\partial}{\partial \xi}(\frac{1}{\bar{x}_\xi}\frac{\partial \bar{u}}{\partial \xi}) + \qquad (2)$$
$$\frac{1}{\bar{y}_\eta}\frac{\partial}{\partial \eta}(\frac{1}{\bar{y}_\eta}\frac{\partial \bar{u}}{\partial \eta})]$$

$$St \cdot \mathrm{Re}\frac{\partial \bar{v}}{\partial \tau} + \mathrm{Re}(\bar{u}\frac{1}{\bar{x}_\xi}\frac{\partial \bar{v}}{\partial \xi} + \bar{v}\frac{1}{\bar{y}_\eta}\frac{\partial \bar{v}}{\partial \eta})$$
$$= -\frac{1}{\bar{y}_\eta}\frac{\partial \bar{p}}{\partial \eta} + [\frac{1}{\bar{x}_\xi}\frac{\partial}{\partial \xi}(\frac{\partial \bar{v}}{\partial \xi}) + \qquad (3)$$
$$\frac{1}{\bar{y}_\eta}\frac{\partial}{\partial \eta}(\frac{1}{\bar{y}_\eta}\frac{\partial \bar{v}}{\partial \eta})]$$

To avoid pressure oscillations, the Marker and Cell (MAC) finite difference scheme in conjunction with a stagger grid was utilized. The mesh in the $\bar{x}$-direction was regenerated after each time step to comply with the movement of the oscillating structure. The velocities and pressure were interpolated from the old mesh into the new mesh accordingly. The mesh in the $\bar{y}$-direction was unchanged during the simulation because the structure did not move in that direction. An explicit finite difference scheme was used to discretize the governing equations. The convection and diffusion terms in the governing equations were central differenced. The nonlinear terms in the finite difference equations were linearized by lagging the coefficients.
The momentum equations, Eq. (2) and (3), were differentiated with respect to $\bar{x}$ and $\bar{y}$, respectively, and added together to obtain a Poisson equation for pressure.

$$\frac{\partial^2 \bar{p}}{\partial \bar{x}^2} + \frac{\partial^2 \bar{p}}{\partial \bar{y}^2} = -St \cdot \mathrm{Re}\frac{\partial \bar{S}}{\partial \tau} -$$
$$\mathrm{Re}\frac{\partial^2 \bar{u}^2}{\partial \bar{x}^2} - 2\,\mathrm{Re}\frac{\partial(\bar{u}\bar{v})}{\partial \bar{x}\partial \bar{y}} \qquad (4)$$
$$-\mathrm{Re}\frac{\partial^2 \bar{v}}{\partial \bar{y}^2} + \frac{\partial^2 \bar{S}}{\partial \bar{x}^2} + \frac{\partial^2 \bar{S}}{\partial \bar{y}^2}$$

where $\bar{S} = \frac{\partial \bar{u}}{\partial \bar{x}} + \frac{\partial \bar{v}}{\partial \bar{y}}$. The expression $\bar{S}^{n+1} = (\frac{\partial \bar{u}}{\partial \bar{x}} + \frac{\partial \bar{v}}{\partial \bar{y}})^{n+1}$ in the $\frac{\partial \bar{S}}{\partial \tau}$ term was set equal to zero, because when the pressure field converges at the n+1 time step the continuity equation should be satisfied.

In the numerical simulations, the Poisson equation, Eq. (4), was solved first

by iteration to obtain the pressure. The convergence criterion for the pressure field was $\sum \left| \overline{p}_{i,j}^{\,k+1} - \overline{p}_{i,j}^{\,k} \right| \le 10^{-4}$, the superscription k is the iteration number. After convergence, the pressure was then substituted into the momentum equations, Eq. (2) and (3), to solve for the $\overline{u}$ and $\overline{v}$ velocities. This completed one time step. This process continued until the periodic steady state was reached. The convergence criterion for the periodic steady state was

$$\sum \left| \overline{u}_{i,j}^{\,n+1} - \overline{u}_{i,j}^{\,n} \right| \le 10^{-4} \qquad (5)$$

where n is the oscillating cycles of the structure. Equation (5) was applied at the beginning of each new oscillating cycle to check for convergence. If the criterion was met then the calculation stopped. This process was time accurate. The computer program was first validated by simulating the Stokes' second problem. The oscillating frequency of the infinite plate was assumed to be $\omega = 8000$ kHz. The numerically calculated shear stresses were compared with the analytical shear stresses at several different time intervals. The difference was less than 1%. The numerically calculated velocity profiles along the $\overline{y}$ -axis at several time intervals were also compared with the analytical solution. The difference was less than 0.6%.

III. Results and discussion

Table 1 compares the analytical, numerical, and experimental Q-factors for the micro comb structure. The oscillation amplitude of the moving electrode was 3d. As demonstrated in Table 3, the numerical simulations subject to the slip boundary conditions show that the contributions to the total damping by the bottom, top, and side surfaces of the oscillating structure are 65.83%, 11.79%, and 12.42%, respectively. The damping on the edge surfaces contributes another 9.94%. The damping on the bottom, top, and side surfaces is due to viscous stress. The damping on the edge surfaces is the result of pressure difference on the right and left surfaces of the oscillating structure, which is induced by the pumping and sucking motions of the moving structure. The bottom surface is the major damping contributor due to the small gap in region II. The top, side, and edge surfaces have approximately equal contribution to the total damping, around 10-12%.

Although the area of the edge surfaces is only 5% of the top surface, the damping of the former is only 16% less than that of the latter. The numerical Q-factor on the bottom surface of the oscillating structure is very close to the analytical Q-factor. This shows that the flow in region II can be modeled by the Couette flow quite well. The numerical Q-factor on the top surface is lower than the analytical Q-factor by about 53%. This means that the numerically predicted damping is higher than the analytical damping by about 114%. The reason was explained in the second paragraph of this section. The slip boundary conditions in region II increase the damping on the bottom surface of the oscillating structure by about 7% but have negligible effect on the damping of the top, side, and edge surfaces.

IV. Conclusions

Numerical results of this study show that the viscous drag on the bottom surface of the oscillating structure is the major contributor of the total damping. It makes up 66% of the total damping for the two micro comb structures investigated. The flow in region II can be modeled and predicted quite well by the Couette flow model. The slip boundary conditions reduce the viscous damping on the bottom surface by about 7%, but have negligible effect on the damping of the other surfaces as were demonstrated in Table 1. The top, side, and edge surfaces each contributes about 10-12% of the total damping. Although the area of the edge surfaces is only 5% of the top surface, it contributes about the same amount of damping as that of the top surface.

References

[1] Y.H. Cho, B.M. Kwak, A.P. Pisano and

R.T. Howe, Viscous energy dissipation in laterally oscillating planar microstructures: a theoretical and experimental study, in: Proceedings of the IEEE Workshop on Microelectromechanical Systems, 1993, pp. 93-98.
[2] W.C. Tang, T.C. Nguyen and R.T. Howe, Laterally driven polysilicon resonant microstructures, Sensors and Actuators, A20 (1989) 25-32.

Table 1: Comparison of analytical, numerical, and experimental Q-factors on different surfaces for the first micro comb structure.

	Top	Bottom	Side	Total
Numerical Q-factors (nonslip)	130.7	21.7	124.1	14.7
Numerical Q-factors (slip)	130.7	23.4	124.1	15.4
Analytical Q-factors (nonslip)	279.6	22.9	124.1	18.1
Experimental Q-factor				14.4

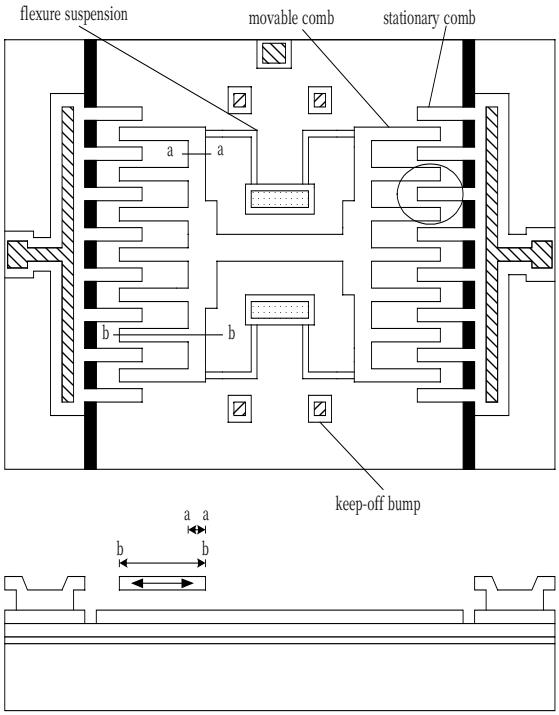

Fig. 1. Schematic diagram of the micro comb structure.